Pergamon

International Journal of Machine Tools & Manufacture 42 (2002) 201–213

INTERNATIONAL JOURNAL OF
MACHINE TOOLS
& MANUFACTURE
DESIGN, RESEARCH AND APPLICATION

# Extension of basic geometric analysis of 3-D chip forms in metal cutting to chips with obstacle-induced deformation

A.G. Kharkevich, Patri K. Venuvinod *

*Department of Manufacturing, Engineering and Engineering Management, City University of Hong Kong, Tat Chee Avenue, Kowloon, Hong Kong*

Received 15 March 2000; received in revised form 13 July 2001; accepted 24 July 2001

**Abstract**

In machining, chips are known to break mainly because of obstacle-induced deformation. Recently, the present authors had reported on a new and basic geometric analysis of 3-D chips in the absence of deformation after separation from the tool rake face. This paper continues the analysis to cover the full lifecycle of chips subjected to obstacle-induced deformation. The main contributions of this paper are the identification of the geometric properties that are likely to be preserved during obstacle-induced chip deformation and their implications, and the utilisation of these properties to obtain insights concerning the geometry of the tool–chip contact area. The new theoretical findings are verified against empirical data obtained through manual deformation of chips, video recordings of the development of obstructed chips, and the use of a specially prepared grooved tool that imposes a predetermined side-curl on the chip. 

## 1. Introduction

Although chip-breaking continues to be a major hurdle in the realisation of unmanned machining, chip-breaker design has remained an art owing to the absence of a systematic theory of chip development [1].

It is generally accepted that initially continuous chips are born curled and may subsequently break owing to the load imposed by an external obstacle such as a tool or work surface [2]. Many researchers have tried to understand the origins of chip forms [3–6] and how one could develop analytical or computational models of the mechanics (principles underlying the loading and deformation patterns) of obstruction-induced chip deformation [7–9].

Geometry is often the key to solving any problem in the field of mechanics—one needs to specify the geometry of the problem *before* attempting to study the loading patterns. However, it appears that our current understanding of the geometry of chips is, at best, sketchy. As a result, previous researchers had to resort to certain arbitrary or empirically inspired geometric simplifications, e.g. restricting the model to 2-D chip forms [7], assuming that an 'ear' type of chip has the form of a spiral with a moving center [8], and/or that the obstacle-induced deformation is purely elastic [8,9].

Irrespective of whether a chip is *free* or *obstructed*, the initial geometry of the chip is decided by the kinematic conditions prevailing at the moment the chip *first* leaves the tool–chip separation line (TCSL). The chip at the TCSL may be called the *original chip* (OC). If the tool rake surface is plane, the TCSL can be expected to be a straight segment.

It appears that current views concerning the geometry of free chips are dominated by those expressed by Nakayama et al. The latter had noted that the generalised trajectory of a particle leaving the TCSL is a 3-D helix that is completely expressible in terms of three parameters associated with the particle's state at the TCSL: up-curl radius ($\rho_u$), side-curl radius ($\rho_s$), and chip flow angle ($\eta$). Nakayama also attempted to analytically express the aggregate geometric parameters (pitch, radius, etc.) of the chip in terms of $\rho_u$, $\rho_s$, and $\eta$ [5]. Subsequently, he viewed the *chip face* (the face that had passed over the TCSL) as a composite of helices and presented diagrams of simulated chip face forms [6]. These diagrams had significant impact on subsequent work in the field.

* Corresponding author. Tel.: +852-2788-8400; fax: +852-2788-8423.
*E-mail address:* mepatri@cityu.edu.hk (P.K. Venuvinod).

0890-6955/02/$ - see front matter 
PII: S0890-6955(01)00115-8

**Nomenclature**

| | |
|---|---|
| $A_0$, $A_1$ | outer and inner points, respectively, of chip face at the ECE |
| $b_{ECE}$ | width of chip along the ECE |
| ECE | equivalent cutting edge as defined in the text |
| $\mathbf{H}_0$, $\mathbf{H}_1$ | outer and inner helices of helical chip face, respectively |
| $\mathbf{H}^c$ | cuspidal helix of helical chip |
| $\mathbf{H}^*$ | helix at the upper boundary of the stretched region of the helical chip face |
| $L_{c0}$ | tool–chip contact length (the arc-distance between the ECE and the TCSL) at the outer edge of the chip |
| $O_0$, $O_1$ | end points of the TCSL generating helix $\mathbf{H}_0$ and $\mathbf{H}_1$, respectively |
| $O_s$ | centre of curvature of the path of a chip particle in the tool–chip contact area |
| $p$ | pitch of helical chip |
| $p_{extr}$ | extreme pitch of helical chip |
| $p_{max}$ | maximum pitch of helical chip |
| TCSL | tool–chip separation line |
| $\mathbf{V}_{A_0}$,$\mathbf{V}_{A_1}$ | velocities of chip particles at $A_0$ and $A_1$, respectively |
| $\mathbf{V}_{O_0}$ | velocity of chip particle at $O_0$ |
| $\mathbf{V}_{O_1}$ | velocity of chip particle at $O_1$ |
| $\mathbf{V}^c_O$ | velocity of chip particle at point of TCSL corresponding to $\mathbf{H}^c$ |
| $x_{O_s}$,$y_{O_s}$,$z_{O_s}$ | coordinates of point $O_s$ in system $XYZ$ |
| $X$, $Y$, $Z$ | right-handed Cartesian axes centred at $O_0$ such that $X$ is directed along the TCSL towards $O_1$ and $Z$ is positively directed outward from the tool rake surface |
| $X^*$, $Y^*$, $Z^*$ | right-handed Cartesian axes centred at $A_0$ such that $X^*$ is directed along the ECE towards $A_1$ and $Z^*$ is positively directed outward from the tool rake surface |
| $\Delta\psi_{(ECE)}$ | angle between the ECE and TCSL |
| $\eta$ | angular deviation of the velocity of a particle at TCSL from the normal to TCSL in the plane of the rake face |
| $\eta_0$, $\eta_1$ | magnitudes of $\eta$ at $O_0$ and $O_1$, respectively |
| $\eta_{0(ECE)}$ | chip flow angles at the outer and inner edges of the chip face, respectively |
| $\eta_{1(ECE)}$ | angle measured on the tool rake plane between the ECE and the normal to the ECE |
| $\theta$ | angle between axis of chip face helix at the tangent line to the cuspidal curve of the chip face and its projection on the tangent plane to the chip face passing through the line (a particular case of this angle was defined in [1]) |
| $\rho$ | radius of a chip-face helix |
| $\rho_s$ | side-curl radius of a chip-face helix |
| $\rho_{s0}$, $\rho_{s1}$ | $\rho_s$ of $\mathbf{H}_0$ and $\mathbf{H}_1$, respectively |
| $\rho_s^*$ | $\rho_s$ of $\mathbf{H}^*$ |
| $\rho_u$ | up-curl radius of chip-face helix |
| $\rho_{u0}$, $\rho_{u1}$ | $\rho_u$ of $\mathbf{H}_0$ and $\mathbf{H}_1$, respectively |
| $\rho^*$ | radius of $\mathbf{H}^*$ |
| $\tau$ | torsion of helix on chip face |
| $\varphi_0$ | angle between $O_sO_0$ and $O_sA_0$ |

However, in Ref. 1, the present authors identified certain inconsistencies in the analyses presented by Nakayama et al. and produced a new analysis based on more plausible definitions of $\rho_u$ and $\rho_s$. Subsequently they extended their analysis to define the geometry of the chip face that could, in turn, be determined from a limited set of dimensional measurements conducted on the resulting *chip-in-hand* (CIH)—chip picked up from the machine's chip collector pan. The analysis also revealed certain geometric constraints governing the development of a chip form.

The work reported by the present authors in Refs. 1 and 2 was limited to free chips, whereas a large proportion of chips produced in industry are obstructed. When a chip meets an obstruction, one can expect the chip form to be subjected to some additional deformation (elastic, or elastic plus plastic) owing to the external load imposed by the obstruction. Consequently, the form of

the chip-in-hand (CIH) will be different from that in the vicinity of the tool–chip separation line (TCSL). However, intuitively, one would expect the deformed chip not to be totally different in form from the initial chip. If so, what would be the geometric properties that would be preserved during the additional deformation of the chip? What are the internal geometric constraints leading to these invariants? This paper aims to explore these apparently 'theoretical' (and, hitherto, unexplored) questions in the belief that the identification of such geometric invariants and constraints, if any, would be of practical value in the analysis of the mechanics of obstructed chips and, eventually, in obtaining a fundamental understanding of the conditions that best promote chip-breaking.

Section 1 of this paper will introduce certain new terms and premises. Section 2 will focus on the analysis of the geometry of obstructed chips after separation from the tool rake face. It will start with the premise that the chip face must be *developable* so as to arrive at definitions of up- and side-curl radii that are more generalised than those presented in Ref. 1. Next, certain geometric properties that, in principle, should be preserved during obstacle-induced deformation will be identified. The section ends with an examination of the implications of these observations with regard to the analysis and measurement of obstructed chips.

Section 3 will examine the tool–chip contact area with the intention of arriving at a complete geometric analysis of the chip face starting with the chip's state at the moment it is born at the primary deformation zone to the time it ends up in the chip collector pan. This analysis is of particular interest because, with the exception of Masuda et al. [10], few researchers seem to have addressed this issue. Further, the analysis in Ref. 10 was limited by the assumption that the chip flow angle is equal to zero everywhere along the equivalent cutting edge. Our new analysis will be free from this limitation.

Section 4 will verify the key theoretical concepts developed in Sections 2 and 3 against experimental data collected through the application of a variety of experimental strategies: manual deformation of chips-in-hand, video recordings of chips-in-process, and the use of circular-groove type chip guides. Finally, Section 5 will summarise the conclusions that can be drawn from Sections 2–4.

## 2. Analysis of the geometry of obstructed chips after separation from the tool

### 2.1. Some new definitions and premises

The analysis to be developed in subsequent sections will be based on several new definitions and premises. In Ref. 1, chips were categorised into lightly obstructed and strongly obstructed types. This categorisation was dictated by considerations relating to the ability of the plastic deformation process within the chip root to adapt to the forces and moments induced by external obstacles. However, we will now utilise a categorisation that is more descriptive from the point of view of the obstacle-induced deformation experienced by the chip after it has passed the TCSL.

It is generally accepted that, in a physical sense, the entity we call a chip is born at the primary plastic deformation zone that emanates from the cutting edge (location E in Fig. 1, adapted from [11]) and spreads towards the junction between the work and chip surfaces. The form of this primary chip is a result of the total deformation the work material had experienced at the zone. However, the primary chip usually experiences 'environmental' influence owing to its interaction with the tool as it traverses the chip–tool contact zone (EC in Fig. 1) so that the 3-D form of its face becomes fully visible only when it arrives at the TCSL. Hence, we may assume that the full form of the generalised 3-D chip is realised only at the TCSL. If the chip happens to meet an intended obstruction such as a clamp-on chip former or an unintended obstruction such as a face of the tool or workpiece, the chip could experience obstacle-induced additional deformation after passing over the TCSL. We may label the chip form after such additional deformation, if any, as the form of the *deformed chip* (DC) while the chip form at the TCSL as the form of the *original chip* (OC).

In situations where the forms of the OC and DC are identical, it can be assumed for all practical purposes

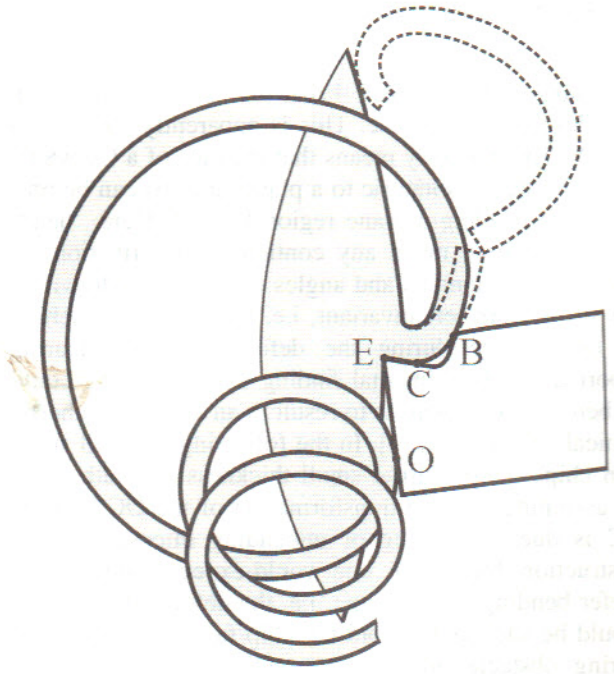


Fig. 1. Chip-in-process (adapted from Henriksen [11]).

that the chip's 3-D form of the chip is fully set at the time of its 'visible' birth at the TCSL. Hence, we may label such a chip as *chip-undeformed-after-separation* (CUAS). Clearly, every CUAS is free or lightly obstructed. However, every lightly obstructed chip may not be a CUAS. A lightly obstructed chip, if it is springy enough, can undergo significant form variation after leaving the TCSL due to obstacle-induced elastic deformation.

A significant difference between the forms of OC and DC indicates the presence of obstacle-induced change in chip form after the TCSL. Hence such a chip may be called a *chip-deformed-after-separation* (CDAS). The analysis presented in Refs. 1 and 2 had addressed only CUAS whereas the present paper extends the analysis to CDAS.

As in Refs. 1, 2 and 4–6, we will assume that the tool rake face is flat at least over the tool–chip contact zone. In general, phenomena within the chip root can be significantly non-stationary particularly because of non-stationary chip–obstacle interaction. However, so as to facilitate the first step in the analysis, we may assume that the phenomena within the chip root are stationary. This implies that the helical geometry of the chip immediately after the chip has passed the TCSL will also be stationary. Such an analysis can be extended to the more difficult case of non-stationary chips by modelling such chips as composites of instantaneously helical OC elements (although the element geometry itself could vary with time) that leave the TCSL and subsequently undergo obstacle-induced deformation.

### 2.2. Idealisation of the face of a chip as a developable surface

Spaans showed in Ref. 4 that the face of a *rigid* chip is a developable surface. This is apparently valid for a CUAS. This property means that the face of a CUAS (i) must be locally isometric to a plane, and (ii) can be produced by *bending* a plane region [12,13]. Here, 'bending' is taken to mean any continuous deformation for which the arc lengths and angles of all curves drawn on the surface are left invariant, i.e. there is no stretching of the surface during the deformation. Pekelharing reported the experimental finding that a flat ring could be bent in such a way as to result in an arbitrarily chosen conical helical form [3]. In the following, we will study thin chips (chips with a small thickness to width ratio) by assuming that the transformation of the OC into the DC is due to bending or unbending imposed by the obstruction. Intuitively, one would expect a thin chip to prefer bending to stretching, i.e. the deformed chip path would be such as to avoid the chip face being stretched during obstacle-induced deformation. It follows from these considerations then that the face of a thin CDAS (hence the face of a thin CIH) is also intrinsically flat and developable.

### 2.3. Generalised definitions of up-curl, side-curl, and chip flow angle

Since the face of a CDAS is a developable surface, it can be represented as a part of the surface swept out by the tangents of a generalised space curve called the *cuspidal curve* [12]. Note that the surface need not always be helical. However, when the face of a deformed chip is helical, the space curve will be a helix. Since the geometry of a CDAS will be different from that of the corresponding original chip (chip at the TCSL), in general, the tangent lines sweeping the face of the DC would be different from those sweeping the face of the OC.

Moreover, irrespective of whether a chip is undeformed or deformed after separation from the tool rake face, one can always identify the *osculating planes* (planes containing the tangent and principal normal lines) of the corresponding cuspidal curve [12]. These planes are tangential to the chip face along the tangent lines to the cuspidal curve and envelope the surface.

Consider now a helical CIH that is also a CDAS. Such a chip can still be formally studied by using the CIH-analysis of CUAS described in Ref. 2. However, in the case of a CDAS, the form of the CIH will be different from that of the chip at the TCSL. As a result, we cannot directly refer to the tool rake plane and the TCSL. However, this problem can be avoided by further generalising the definitions of $\eta$, $\rho_u$, and $\rho_s$ given in Ref. 1. The generalisation can be achieved by referring to the tangent plane of the deformed chip face and to the straight line along which the tangent plane contacts the chip face. This reinterpretation leads to the following definitions of up-curl and side-curl curvatures and radii, and chip flow angles applicable to both *helical* chips with and without obstacle-induced deformation:

1. The side-curl curvature at a point on the chip face is the vector projection of the curvature of the chip face helix passing through the point onto the tangent plane of the chip face at that point (since chip side-curl takes place in a plane tangential to the chip face). The side-curl radius ($\rho_s$) is equal to the reciprocal value of the magnitude of the side-curl curvature.
2. The up-curl curvature at a point on the chip face is the vector projection of the curvature of the chip face helix passing through the point onto the normal vector to the chip face at that point (and hence onto the normal vector to the tangent plane to the chip face at that point). The up-curl radius ($\rho_u$) is equal to the reciprocal value of the magnitude of the up-curl curvature.
3. The chip flow angle ($\eta$) at a point on the chip face is measured in the tangent plane at the point to the chip face and is defined as the angle between the tan-

gent to the chip face helix passing through the point and the normal to the line of contact between the tangent plane and the chip face.

In the general case when the form of a CDAS is not helical and the chip formation is not stationary (although the cut width is constant), definitions (i) to (iii) would need to be further generalised by substituting the clause 'the chip face helix passing through the point' with 'the curve on the face that is parallel (in the sense of intrinsic geometry of the surface) to the edges of the chip face and passing through the point'.

### 2.4. Geometric features preserved during the deformation of the chip face

According to Section 2.2, the face of any segment of a CDAS (a DC) and the segment of this chip at the TCSL (the OC) are intrinsically flat and isometric. Therefore *all the intrinsic properties of the face of the original and deformed chips must be identical* [14]. This principle should be applicable even if the tool rake face is curved.

The *geodesic curvature* of a curve on a surface at a point of the curve is the vector projection of the curvature vector of the curve at the point onto the tangent plane to the surface at the point [14]. This parameter defined along a curve on a surface is an intrinsic property of the surface. Therefore, the geodesic curvature of a chip face curve is likely to be preserved under obstacle-induced chip deformation.

The above definition of geodesic curvature coincides with that of side-curl curvature postulated in the previous section provided that we interpret 'a curve' as 'a chip face helix' (or a curve on the face that is parallel to the edges of the chip in the generalised case of a CDAS) and 'the surface' as 'the chip face'. This implies that the geodesic curvature of the chip face curve at a point on the curve is equal to the side-curl curvature at that point. Consequently, the side-curl curvature (as well as the side-curl radius) at a point on a chip face must be preserved during any subsequent deformation of the chip. Therefore the side-curl curvature at a point of a CDAS is likely to be equal in magnitude to that of the OC at the point. Thus, if we apply the CIH-analysis developed in Ref. 2 to a helical CIH that is also a CDAS, the side-curl radii determined through such an analysis are likely to be equal in magnitude to those of the corresponding chip at the TCSL.

### 2.5. Determining chip face geometry from parameter set ($\rho_{u0}$, $\rho_{s0}$, $\rho_{u1}$, $\rho_{s1}$)

According to Ref. 1 and Section 2.4 above, a helical chip face can be completely defined by any one of a variety of parameter sets: ($\rho_0$, $\rho_1$, $p$, $h_1$), ($\rho_o$, $\eta_o$, $\theta$, $L_1$), ($\rho_o$, $\eta_o$, $\eta_1$, $\theta$), and ($\rho_{u0}$, $\rho_{s0}$, $\eta_o$, $\eta_1$), etc. However, it is more advantageous to utilise the last set, ($\rho_{u0}$, $\rho_{s0}$, $\rho_{u1}$, $\rho_{s1}$), because the four parameters in this set are homogeneous and at least two of them are likely to be preserved as the chip experiences progressive deformation during a chip's life cycle. This parameter set is easily determined using equations (20b) and (26) in Ref. 1 and equation (2) in Ref. 2:

$$|\eta_0| = \sin^{-1}\sqrt{\frac{\left(\frac{\rho_{u0}\rho_{s1}}{\rho_{u1}\rho_{s0}}\right)^2 - 1}{\left(\frac{\rho_{u0}\rho_{s1}}{\rho_{u1}\rho_{s0}}\right)^2 - \left(\frac{\rho_{s0}}{\rho_{s1}}\right)^2}} \tag{1}$$

and

$$\eta_1 = \sin^{-1}\left(\frac{\rho_{s0}}{\rho_{s1}}\sin\eta_0\right) \tag{2}$$

The above equations enable us to transit from set ($\rho_{u0}$, $\rho_{s0}$, $\rho_{u1}$, $\rho_{s1}$) to set ($\rho_{u0}$, $\rho_{s0}$, $|\eta_0|$, $|\eta_1|$).

It follows from the above that any deformation of a chip face can be viewed as a combination of specific changes in the planes of side curl and up-curl that, in turn, can be expressed in terms of changes in just the up-curl curvatures/radii.

An important implication of Eq. (1) is the necessity of the following condition being satisfied:

$$\frac{\rho_{u1}}{\rho_{u0}} \geq \frac{\rho_{s1}}{\rho_{s0}} \text{ when } \rho_{s1} \leq \rho_{s0} \tag{3}$$

However, the parameter set ($\rho_{u0}$, $\rho_{s0}$, $\rho_{u1}$, $\rho_{s1}$) completely determines the magnitudes but not the signs of $\eta_o$ and $\eta_1$. This implies that the chip flow angle is related not merely to the curvature of the chip face helix but also to some other parameter(s). What could it/they be? To answer this question, we need to consider the significance of torsion, $\tau$, of the chip face helix:

$$\tau = \frac{\tan\eta}{\rho_u} \tag{4}$$

Since, usually, $\rho_u$ is positive, Eq. (4) implies that the signs of $\tau$ and $\eta$ will normally be the same. Hence, it is plausible that the key parameter influencing the sign of $\eta$ of a chip face helix is its torsion, $\tau$.

It is useful to note that $\tau$ determines the pitch of the chip and how a helix on the chip face is positioned in space with respect to adjacent helices on the chip face. Further, along with the curvature of a helix, torsion determines the curvature of the chip face. However, Eqs. (1), (2) and (4) stipulate a certain relationship between the torsion of a helix and the distribution of the curvature of the helices across the chip face. As a result, it is possible to determine the torsion merely from the magnitudes of $\rho_{u0}$, $\rho_{s0}$, $\rho_{u1}$, and $\rho_{s1}$.

### 2.6. Obstacle-induced chip deformation is a two-degree of freedom process

Parameter set ($\rho_{u0}$, $\rho_{s0}$, $\rho_{u1}$, $\rho_{s1}$) enables us to effectively apply the principle of preservation of intrinsic properties of chip face during our analysis of chip deformation. One can easily show on the basis of the previous discussion that, in contrast to side-curl radii, up-curl radii are not intrinsic properties of the chip face and therefore they can vary independently (thus representing different chip face deformations). Hence, in general, chip deformation is essentially realised through the two degrees of freedom represented by the two up-curl radii, $\rho_{u0}$ and $\rho_{u1}$.

It appears that the degree of influence of an obstacle-induced deformation on any one of the various geometric parameters of the chip face is related to the magnitudes of the side-curl radii that have been inherited from the chip at the TCSL and have remained intact during any subsequent obstacle-induced deformation. Figs. 2(a) and (b) respectively show how $\eta_0$ and $\eta_1$ vary under different curl ratios $\rho_{s1}/\rho_{s0}$ and $\rho_{u1}/\rho_{u0}$. Note that Eqs. (1) and (2) imply that the chip flow angles do not change at all if $\rho_{u1}/\rho_{u0}$ is held constant during the deformation. The angles become smaller very rapidly when $\rho_{u1}/\rho_{u0}$ approaches the extreme value $\rho_{s1}/\rho_{s0}$. When $\rho_{u1}/\rho_{u0}=\rho_{s1}/\rho_{s0}$, we have $\eta_0=\eta_1=0$. This observation, in turn, implies that the torsion and the pitch of the chip must be equal to zero.

In contrast to chip flow angles $\eta_0$ and $\eta_1$, pitch $p$, radii $\rho_0$ and $\rho_1$, and angle $\theta$ are sensitive not just to the change in $\rho_{u1}/\rho_{u0}$ that might result from chip deformation. It is found that (see Figs. 3(a), (b) and (c)), when $\rho_{u1}/\rho_{u0}$ (and thus $\eta$) is held constant, these parameters are also sensitive to possible independent changes in $\rho_{u0}$ and $\rho_{u1}$.

The finding that *two* independent parameters, $\rho_{u0}$ and $\rho_{u1}$, are sufficient to characterise helical chip deformations has some noteworthy implications. Firstly, it means that the deformation of the OC cannot be described in terms of a change in the pitch or radius of the chip alone. This is because an infinite variety of deformed chips with the same pitch but different external radii can be obtained from the same OC. Similarly, there exist an infinite variety of possible deformed chips with the same external radius but different pitches. Among these deformed chips, there would only be one exhibiting a particular combination of pitch and external radius that can be obtained from the OC through additional deformation.

The presence of two degrees of freedom of deformation of a helical chip is clearly apparent when we conduct a simple experiment by taking an annulus cut from a flat sheet of celluloid and subjecting it to deformation (manually or otherwise). Interestingly, a conical helical form (but never a tubular helical form) with values of pitch and external radius varying in a wide range can be obtained in such an experiment. (Note that, according to the theory developed above, the finite inner and outer radii of the annulus would be equal to the corresponding radii of side curl of the modelled helical chip whereas the side-curl radii of a tubular helical chip are infinite in magnitude.) Similar experiments conducted with a straight flat ribbon also demonstrate that it is possible to obtain a variety of tubular forms exhibiting

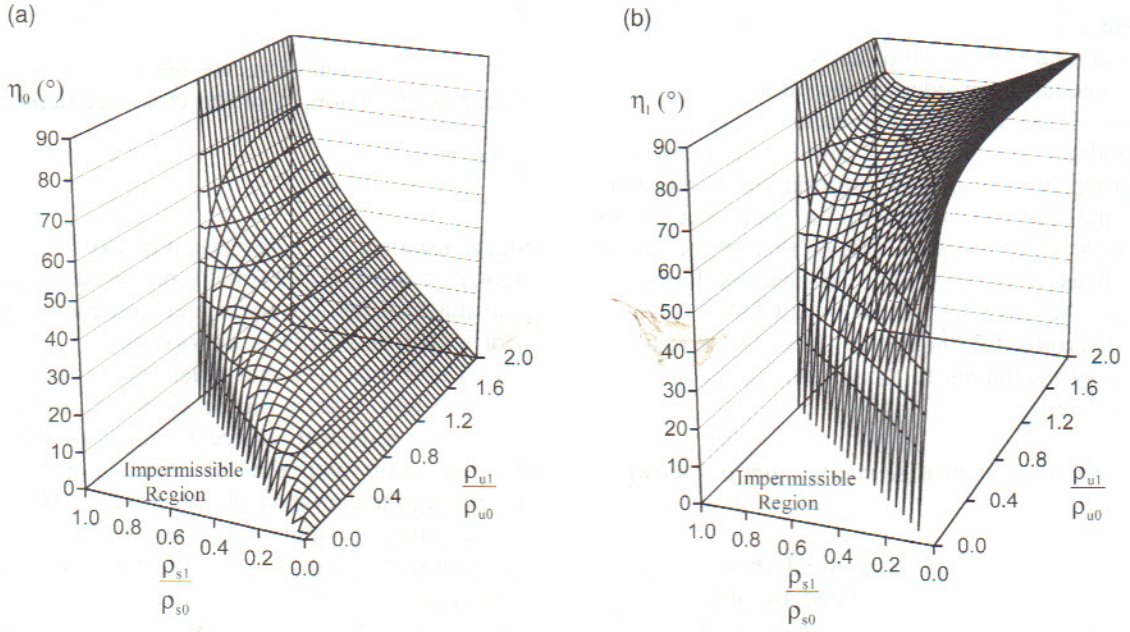


Fig. 2. Chip flow angles $\eta_0$ and $\eta_1$ as functions of the ratios of up- and side-curl radii.

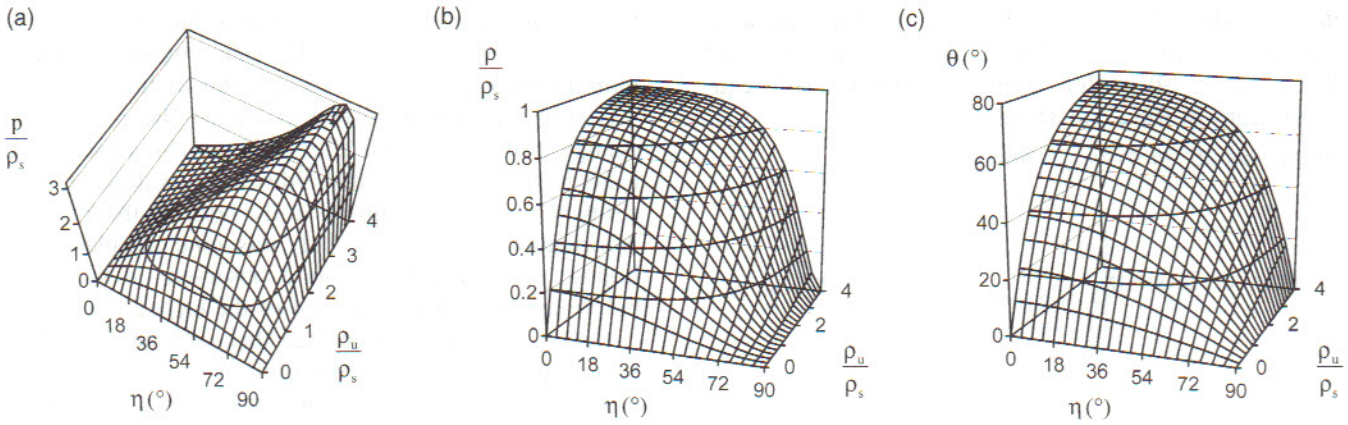


Fig. 3. Pitch of chip $p$, radius $\rho$, and angle $\theta$ as functions of chip flow angle and the ratio of up-curl radius to side-curl radius.

a range of values of pitch and external radius but never a conical helical form. These observations lend credibility to the arguments underlying the assertion that side-curl curvature is preserved during the deformation of a thin chip under the influence of an external obstacle.

### 2.7. Possible annihilation of up-curl curvature at the inner side of the chip face

It was shown in Ref. 2 that $\eta_0 \leq \eta_1$ for a CUAS and, hence, for a deformed helical chip (CDAS). Consequently, during a deformation (e.g. while subjecting a chip to tension so as to increase its pitch), $|\eta_1|$ tends to reach 90° first. However, when this happens, following equation (20a) in Ref. 1, the chip up-curl radius, $\rho_{u1}$, will approach infinite magnitude. This means that (i) the up-curl curvature of a conical helical chip can be completely annihilated through subsequent deformation, and (ii) when this happens, it would first occur at the inner edge of the chip. Further deformation of the chip can be produced only through changes in the up-curl curvatures of the outer helical fibres of the chip face (since the side-curl curvature of chip is likely to remain unchanged during deformation). Consequently, the up-curl curvatures of the chip face fibres adjacent to the extreme inner fibre will progressively decrease and, finally, disappear altogether after sufficient further deformation.

The above theory suggests that, when $|\eta_1|$ reaches 90° (i.e. when the innermost fibre has lost its up-curl curvature completely), further deformation of the chip will occur through a process where the annihilation of up-curl curvature gradually spreads from the inner edge to the outer edge of the chip face. The authors observed the occurrence of this phenomenon when they studied some metal cutting chips-in-hand of the corkscrew type. This spreading process implies that, in time, a strip of chip with zero up-curl curvature will appear in the vicinity of the inner edge of the chip. Let us designate the helix at the outer boundary of the strip as **H*** and the corresponding helix radius as $\rho^*$. Once $|\eta|$ has reached its maximum value (90°) in the region, further chip deformation there (such as that associated with a change in the pitch of the chip face) can be effected only through a change in the side-curl curvature. This should cause a gradual stretching of the chip face in the region that is maximal at the inner edge of the chip. The stretching means that the chip face portion is no longer developable. This is how the pure side-curled part of the chip is able to have a non-zero pitch that is impossible in case of the intrinsically flat chip face.

### 2.8. The extreme pitch of a helical chip

It can be shown that the pitch of the bounding helix with radius $\rho^*$ is given by

$$p = \frac{2\pi\rho_s^*}{\tan\theta + 1/\tan\theta} \tag{5}$$

It follows from the above equation that the pitch reaches its maximum when $|\theta| = 45°$ and this maximum pitch is given by

$$p_{max} = \pi\rho_s^* \tag{6}$$

Consequently, to the extent that the principle of preservation of the original side-curl curvature is applicable to a CDAS, the pitch of the chip is limited by its maximum side-curl radius. Hence we may introduce the notion of extreme pitch ($p_{extr}$) for each helical chip where

$$p_{extr} = \pi\rho_{s0} \tag{7}$$

However, experimental observations have shown that a stretched chip rarely reaches the extreme pitch because the stretching of the chip face causes the chip to break well before the stretched region has reached the outer edge.

Note that the extreme pitch referred to in Eq. (7) can be estimated directly from the principle of preservation

of chip side-curl curvatures/radii; i.e. without considering up-curl annihilation. This is apparent from the fact that equation (9) in Ref. 1 can be combined with equation (20b) in Ref. 2 to show that

$$p=\pi\rho_s \sin 2\theta \sin\eta \Rightarrow p_{extr}=\max(p)$$

$$=\pi\rho_s \sin 2\theta \sin\eta\Big|_{\substack{\rho_s=\max(\rho_s)\rho=s0 \\ \sin 2\theta \sin\eta=\max(\sin 2\theta \sin\eta)=1}} =\pi\rho_{s0}$$

The above finding suggests that it should be possible to restrict the pitch of a helical chip by deliberately imposing an appropriate magnitude of side-curl curvature on the chip at the TCSL. This observation should be of practical value in chip control.

## 3. Tool–chip contact geometry

### *3.1. The contrasting appearances of chip side-curl and up-curl*

The present analysis assumes that the up-curl curvature of a chip face is born at the primary deformation zone but this is only a 'latent' birth. In other words, although the chip is born up-curled, owing to some phenomenon, the chip face up-curl does not become fully visible until the chip has been separated from the tool rake face at the tool chip separation line.

In contrast to Hahn's work [15] (and many subsequent works) that had validated the 'chip is born curled theory' for pure up-curled chips, the present paper is concerned with origin and nature of 3-D chip curvature. Moreover, the new theory encompasses strongly obstructed chips that have been deformed plastically after exiting from the tool rake face.

So far, we have analysed the behaviour of chip up- and side-curl curvature components during a part—the stage after exiting from the TCSL—of the lifecycle of obstructed chips, in particular, strongly obstructed ones. The analysis has revealed that the side-curl curvature is likely to be preserved whereas the up-curl curvature can be changed. As already explained, the up-curl curvature of the chip face within the tool–chip contact area is only 'latent'. This leads to the following important question: Is the side-curl curvature of a chip at the TCSL affected by plastic deformation of the chip's local layers within the secondary deformation zone over the tool–chip contact area? Or, is the side-curl curvature fully developed immediately after the primary deformation zone?

In order to be able to answer the above question, the present authors repeated Hahn's chip-etching experiments on some tubular chips (mainly up-curled chips), conical helical chips (chips with comparable magnitudes of up-curl and side-curl curvatures), and corkscrew chips (mainly side-curled chips). The tests included strongly obstructed chips obtained while machining steel and aluminium workpieces. The experimental finding on every 3-D chip was similar to that of Hahn—there was little change in the chip form after etching. This observation leads to the conclusion that side-curl curvature of even strongly obstructed chips is fully born at the primary deformation zone because only this zone can plastically impose the side-curl curvature observed on the chips before the etching into the rest of the etched chip body.

Hence, we may assume then that side-curl curvature of a chip is fully born at the primary deformation zone itself whereas the up-curl curvature is in a latent state until the chip has exited from the tool–chip contact area. This assumption seems to hold even in the presence of a secondary flow layer or kinematical dead zone since, as shown in Refs. 16 and 17, the height of this layer is quite small compared with the chip dimensions. The following sections will show that the hypothesis leads to several interesting conclusions regarding the shape and size of the tool–chip contact area associated with the generalised helical form of 3-D chips.

### *3.2. Circular path of a chip face particle over the tool–chip contact area*

Consider now the geometry of the tool–chip contact area—the area between the TCSL and the equivalent cutting edge (ECE). (The ECE is defined for a multiple edge cutting operation as the line joining the two end points of the intersection line or curve segment between the upper boundary of the primary deformation zone and the tool rake face.)

Fig. 4 shows the top view of the flat tool rake with the chip face lying over the tool–chip contact area. Straight line $A_0A_1$ is the ECE and points $A_0$ and $A_1$ are

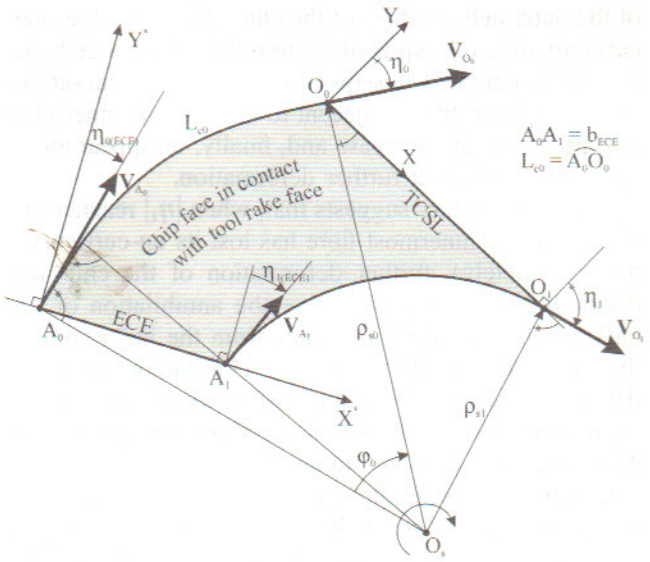


Fig. 4. Geometry of chip face in contact with tool rake face.

the extreme points of the chip face at the ECE. Chip particle velocities, $\mathbf{V}_{A_0}$ and $\mathbf{V}_{A_1}$, are directed in some directions parallel to the tool rake plane.

It can be shown that all particles of the 3-D chip face along the TCSL ($O_0O_1$), exhibit the same centre of side-curl curvature on the tool rake plane, $O_s$, such that

$$x_{O_s}=\frac{\rho_o \cos\eta_0}{\sin\theta\sqrt{1-\sin^2\eta_0\cos^2\theta}} \tag{8a}$$

$$y_{O_s}=\frac{\rho_o \sin\eta_0}{\sin\theta\sqrt{1-\sin^2\eta_0\cos^2\theta}} \tag{8b}$$

Therefore, all chip particles at the TCSL can be viewed as undergoing an instantaneous rotation parallel to the tool rake plane around the common centre of the curvature. Since the chip body can be assumed to be quasi-rigid in the tool–chip contact area and has been formed after the work material has crossed the upper boundary of the primary deformation zone (or the ECE), velocities $\mathbf{V}_{A_0}$ and $\mathbf{V}_{A_1}$ are velocities of stationary rotation of the chip particles around $O_s$ at the moment they arrive at the TCSL. Consequently, except in the extreme case when the radius of the chip rotation of each chip face particle is equal to infinity, there can be no translation in the movement of the chip face particles up to the TCSL.

Note that chip-in-process images implying non-circular or non-straight contours of the tool–chip contact area are sometimes observed. However, this usually happens only when chip formation at the primary deformation zone is non-stationary such that the primary deformation zone produces a time-varying chip side-curl or chip flow direction. This explanation is confirmed by the empirical observation (in experiments conducted by the present authors) that whenever a non-circular chip contour was implied the corresponding CIH was not uniform. For the present, we consider only the stationary case. Therefore, the path of the chip face particle at the tool–chip contact area is circular with the radius equal to the side-curl radius of the chip face whereas the tool–chip contact area is bounded by straight lines of the ECE, TCSL, and two circular arcs with the radii equal to the side-curl radii of the outer and inner edges of the helical CIH.

### 3.3. Chip flow angles at the ECE: $\eta_{0(ECE)}$ and $\eta_{1(ECE)}$

Following Fig. 4, it can be shown that

$$\eta_{1(ECE)}=\cos^{-1}\left(\frac{\left(\frac{\rho_{s0}}{b_{ECE}}\right)^2-\left(\frac{\rho_{s1}}{b_{ECE}}\right)^2-1}{2\frac{\rho_{s1}}{b_{ECE}}}\right) \tag{9}$$

and

$$\eta_{0(ECE)}=\eta_{1(ECE)}-\cos^{-1}\left(\frac{\left(\frac{\rho_{s0}}{b_{ECE}}\right)^2+\left(\frac{\rho_{s1}}{b_{ECE}}\right)^2-1}{2\frac{\rho_{s0}\rho_{s1}}{b_{ECE}^2}}\right) \tag{10}$$

Thus, if $\rho_{s0}$, $\rho_{s1}$ and $b_{ECE}$ are already known, $\eta_{0(ECE)}$ and $\eta_{1(ECE)}$ can be calculated.

### 3.4. Angle $\Delta\psi_{(ECE)}$

$\Delta\psi_{(ECE)}$=(ECE;TCSL). Knowledge of the angle is important while translating insights obtained with regard to the geometric state of the chip at the TCSL to the ECE.

It follows that:

$$\Delta\psi_{(ECE)}=\varphi_0+\eta_{0(ECE)}-\eta_0 \tag{11}$$

Note that, since $\varphi_0=L_{c0}/\rho_{s0}$, $\eta_0=\eta_{0(ECE)}-\Delta\psi_{(ECE)}$ (this equation was stated earlier in Ref. 6) only if $L_{c0}=0$ or $\rho_{s0}=\infty$. For example, when $L_{c0}=0.6$ mm, $\rho_{s0}=2.5$ mm, $\eta_{0(ECE)}=0°$ and $\Delta\psi_{(ECE)}=0°$, we obtain $\eta_0=13.75°$ in contrast to the zero value following the equation suggested in Ref. 6.

## 4. Experimental verification of the analyses presented in Sections 2 and 3

### 4.1. Studies involving manual deformation of helical chips

These experiments involved manual deformation of helical chips. The chip loading modes included axial compression, axial tension, and torsion. Four chip-in-hand samples were collected from chips produced in cylindrical turning of steel workpieces using a carbide tool with a flat rake face and a clamp-on chip former. The cutting conditions and the chip former orientation with respect to the cutting edge were varied so as to obtain chips of different forms.

During our early attempts at manually deforming real chips (both axial load and torsion were tried), it became clear that the outer and inner radii of the chips could be changed only marginally. Hence, subsequent experiments were directed towards just changing the pitch of each sampled chip so as to achieve the maximum possible change in pitch. Chips loaded beyond the deformation limit exhibited quick breakage.

The original chips-in-hand as well as the corresponding manually deformed chips were subjected to the chip-in-hand analysis described in Ref. 2 for chips-undeformed-after-separation and extended in Section 3 above to chips-deformed-after-separation. The parameter set

($\rho_0$, outside radius; $\Delta\rho$, the difference between the outer and inner radii; $|p|$, the absolute value of the pitch; $|h_1|$, the axial length of the chip face) was measured for each chip sample. The measurements were repeated several times at different locations on each chip so as to obtain statistically significant results. The CIH-analysis enabled calculation of the corresponding values of the side-curl curvatures and up-curl curvatures of the chips.

An initial examination of chip measurement data revealed significant scatter. Further analysis of the data indicated that the observed variations in the dimensions of the original and deformed chips were composed of regular (periodic) as well as random components so that we could assume that the sampled data were distribution-free. Hence, the *midrange* and the corresponding *range* were used instead of the traditional mean and standard deviation for statistical representation of the data [18].

On the whole, the differences between the midrange values of the side-curl curvatures of the original and the corresponding deformed chips remained within 7% of the corresponding midrange values of the total curvatures of the original chips. This was true with regard to both the outer and inner chip helices. The observed differences between the midrange values of the side-curl curvatures were about half of the maximum values that could be caused by deviations of the side-curl curvatures due to the irregularity of chip geometry (as estimated from the ranges).

In contrast, the differences between the midrange values of the up-curl curvatures of the original and the corresponding deformed chips were up to 27% of the corresponding midrange values of the total curvatures of the original chips. The observed differences between the midrange values of the up-curl curvatures were about twice the maximum values that could be caused by deviation of the up-curl curvatures due to the irregularity of chip geometry. Clearly, these observations support the hypothesis of side-curl curvature preservation.

### 4.2. Video recording of chips-in-process

This set of experiments involved video recording of the chip segment in the vicinity of the TCSL. The visual images were recorded using a commercially available video camera capable of capturing image frames at intervals of 40 ms. The digitised video-signals were passed to a computer by means of a capture board.

Turning experiments were performed on a horizontal lathe using a high-speed-steel tool with a flat rake face. The tool nose radius was selected to be zero so as to avoid difficulties in locating the equivalent cutting edge. A wedge type chip-former clamped on the tool rake face was used to guide chips such that a variety of long helical chip segments could be obtained. The work material used was mild steel and the cutting speeds were 0.5 m/s and 1.6 m/s.

The video camera, which was equipped with a strong enough zoom lens, was placed at an appropriate distance above the cutting tool to capture views parallel to the tool reference plane of the chip-in-process in the vicinity of the TCSL. Sometimes, an additional video camera was used to record the auxiliary view of the cutting zone from one side in a plane perpendicular to the tool reference plane.

Figs. 5(a)–(c) show three examples of video images collected from three distinct types of turning operations. Together, these three examples cover a fairly wide range of combinations of chip flow angle and up- and side-curl curvatures. The chip in Fig. 5(c) is approximately tubular, i.e. its total curvature is dominated by up-curl curvature whereas the side-curl curvature is close to zero. The chip in Fig. 5(a) represents the other extreme since this is a corkscrew type of chip and, for such a chip, the up-curl curvature is very small so that the total curl is dominated by side-curl. The chip in Fig. 5(b) is of an intermediate form since it is a conical helical chip. Such a chip has comparable magnitudes of up- and side-curl curvatures.

The main motivation behind the collection of the video images in Fig. 5 was to anticipate the broad geometric features of the chip segment in each video image on the basis of a finite set of measurements conducted on the corresponding CIH. If the anticipated features had indeed matched the features actually observed in the video images, one would have verified the theoretical analysis presented in Section 2. A computer simulation program was developed for facilitating this matching task.

An examination of the video recordings revealed that each of these chips had encountered an external obstacle. Thus, none of the chips shown in Fig. 5 could be a free chip—each had to be an obstructed chip. Each of these chips was subjected to a detailed analysis with the help of the simulation program referred to earlier. During the analysis, special attention was paid to the identification of the corresponding portions of the chip-in-hand as well as the chip-in-process. The final magnitudes of some important parameters determined by the simulation program are shown below each chip image.

The following common conclusions could be drawn from these experiments:

1. The projections of the chip flow circles on the tool reference plane in the vicinity of the ECE matched well with the actual edges of the chip in that vicinity (see Fig. 5). This indicated that the side-curl radii of the chips-in-process were the same as those of the chips-in-hand.
2. The simulated $b_{ECE}$ values were plausible (they were slightly larger than the width of the equivalent cutting edge estimated from the idealised cut geometry).
3. The chip flow angles output by the simulation exer-

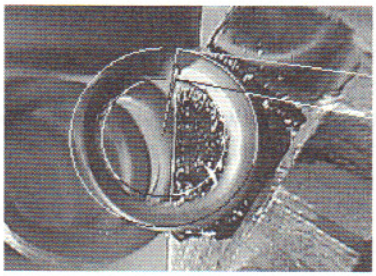

(a) $\rho_{s0} = 5.4$ mm, $\rho_{s1} = 3.6$ mm
$\eta_{0(ECE)} = 6.4^{\circ}$, $\eta_{1(ECE)} = 9.7^{\circ}$

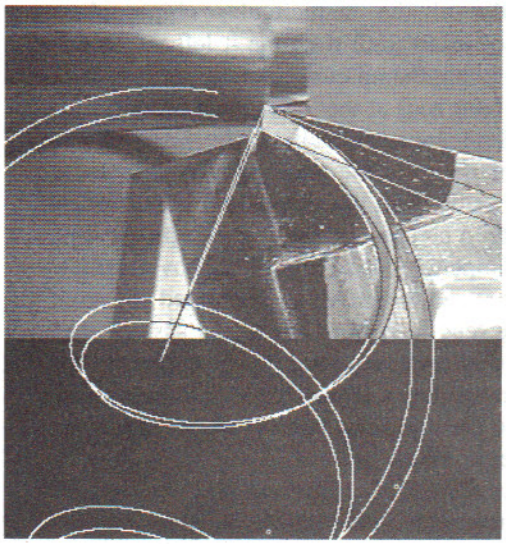

(b) $\rho_{s0} = 16.7$ mm, $\rho_{s1} = 15.4$ mm
$\eta_{0(ECE)} = 11.4^{\circ}$, $\eta_{1(ECE)} = 12.4^{\circ}$
$\rho_{u0} = 12.7$ mm, $\rho_{s1} = 11.9$ mm
$L_{c0} = 0.6$ mm

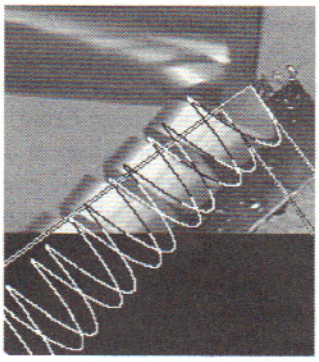

(c) $\rho_{s0} = 164.2$ mm, $\rho_{u1} = 161.9$ mm
$\eta_{0(ECE)} = 4.25^{\circ}$, $\eta_{1(ECE)} = 4.31^{\circ}$
$\rho_{u0} = 3.20$ mm, $\rho_{u1} = 3.16$ mm
$L_{c0} = 0.2$ mm

Fig. 5. Analysis of video images of chips-in-process.

cises were close to the angles of inclination of the corresponding ECE—in agreement with the well-known Stabler's rule.

In addition, for the chip shown in Fig. 5(b), the simulated magnitudes of up-curl radii output by the simulation program for the CIP were found to be significantly smaller than the corresponding magnitudes of the CIH. As for the chip shown in Fig. 5(c), it was found that within the CIP-segment between the TCSL and the workpiece, there was a transition of the up-curl radii from the values at the TCSL to slightly bigger values of the CIH leading to the offset of the tubular chip axis.

The above findings broadly verify the theory presented in Section 2. They also indicate that the new theory enables us to obtain deeper insights into the nature of chip form generation than has been possible hitherto.

### *4.3. Experiments with a specially designed circular chip guide*

One way of more directly verifying the principle of preservation of side-curl curvatures/radii is to test the principle on a side-curled CIP with a known side-curl at the TCSL in a situation when the form of the corresponding CIH has apparently different geometry—thus indicating the presence of significant obstacle-induced deformation. This was exactly the aim of the current experimental work.

The experiment involved the use of a specially designed square carbide tool insert that had a semicircular groove with its axis orthogonal to the insert's rake plane. The groove's cross-section was rectangular with the base-width equal to 2 mm. The bottom edge of the groove acted as the cutting edge.

The insert was used to perform a longitudinal turning operation on a cylindrical workpiece with a tubular end such that the entire wall thickness of the tube was machined in one pass. The wall thickness was set at 1.3 mm so as to be sure that it was sufficiently smaller than the width of the groove so as to avoid chip clogging while still enabling the groove to guide the chip flow path. The insert was so set as to ensure that the cutting edge was orthogonal to the cutting speed (the edge was parallel to the workpiece radial direction).

An examination of the video ascertained that the chip

had indeed followed the semicircular chip-guiding groove of the tool insert until the time it left the insert. One could assume that the up-curl curvature of the chip-in-process was about zero at the TCSL because the chip face had been kept approximately at the level of the groove bottom plane up to the zone of chip–workpiece collision located aside from the tool insert. Moreover, it was observed after a certain cutting time had passed that the chip had completely filled up the groove section (from wall to wall) although it had continued to move along the groove length. Hence, one could assume that the CIP was steady and was purely side-curled at the TCSL with the magnitudes of its side-curl radii $\rho_{s0}$ and $\rho_{s1}$ being close to the outer and inner radii of the groove walls and, hence, constant.

Although the chip had remained essentially flat throughout its journey along the groove in the tool insert, it had acquired a significant magnitude of pitch later (about 7.6 mm). An examination of the video images showed that this was the result of the chip being obstructed by the unmachined surface of the rotating workpiece. The workpiece had pulled the chip down and induced additional plastic deformation. Thus, in this experiment, the form of the CIH was strongly obstructed and, hence, its form was quite different from that it had at the TCSL.

Upon closer examination, the CIH exhibited a certain degree of irregularity. This indicated that the chip's encounter with the unmachined work surface (the external obstacle) was somewhat variable in nature. As a result, considerable care had to be taken during the measurement of the chip's dimensions—the measurements had to be repeated several times according to a carefully devised plan. The best estimates of CIH dimensions thus arrived at were used to calculate the side-curl radii of the CIH. The calculations yielded the following estimates for the side-curl radii of the chip-in-hand: $\rho_{s0}$=4.23–4.43 mm, and $\rho_{s1}$=2.57–2.87 mm. Note that these magnitudes are quite close to the corresponding dimensions (outer radius=4.5 mm, and inner radius=2.5 mm) of the chip guiding groove. This finding unambiguously supports the principle of preservation of the side-curl curvature developed in Section 2.

## 5. Summary and conclusions

A geometric analysis of the deformed chip face has been presented with the aim of identifying the geometric parameters of the face that are likely to be preserved during the chip's transition from its original state at the TCSL to its subsequent deformed state. It has been found that all intrinsic properties of chip face are likely to be preserved.

An important outcome of the analysis is that the definitions of side-curl and up-curl curvature/radius and flow angle of 3-D chip face have been generalised. These definitions are applicable to the faces of chips-deformed-after-separation as well as to chips-undeformed-after-separation. The new analysis has, in effect, extended the CIH-analysis developed in Ref. 2 to encompass chips-deformed-after-separation.

The new analysis leads to the following conclusions of practical importance:

- The side-curl curvatures and radii of a chip are likely to be preserved during obstacle-induced additional deformation of the chip after its separation from the tool rake face.
- There exist only two degrees of freedom while a chip, after its separation from the tool, adapts to the loads imposed by an encounter with an external obstacle.
- In some cutting situations, there exists the possibility of the up-curl curvature being annihilated during obstacle-induced deformation of a chip. This annihilation process occurs through stretching of the chip face that can be expected to begin at the inner edge of the deformed chip and proceed towards the outer edge. Chip breaking occurs when the degree of stretching is excessive.
- The principle of preservation of side-curl curvatures/radii implies that there exists a maximum limit on the possible pitch of a helical chip and this limit depends on the magnitude of the side-curl curvature/radius of the chip.

Future research into chip control could profitably utilise the above findings.

While up-curl curvature of the chip face is not visible until the chip has exited from the TCSL, the side-curl curvature of an initially continuous chip is likely to be constant and visible along the entire tool–chip contact area. Based on this premise, expressions have been developed for the important geometric parameters related to the chip face over the entire tool–chip contact area. These expressions complete the theoretical foundation required for the geometric analysis of the chip face starting from its state when it was born at the primary deformation zone to the state in which it ends up in the chip collector pan of the machine.

The new extended geometric analysis has been verified against data collected from a variety of experiments. Experiments involving manual deformation of chips-in-hand have not negated the hypothesis of preservation of side-curl curvature—thus showing that the hypothesis is plausible.

Studies on the video images of CIP representing the wide range of possible combinations of up-curl and side-curl curvature have indicated that the simulation program developed on the basis of the new theory is capable of anticipating the actual form of the CIP from the corresponding CIH quite well. Since the principle of preser-

vation of the side-curl curvature of the chip face is an important component of the theory developed in the present paper, it can be concluded that this principle has been verified. Further, the new theory merely extends the geometric analyses presented in Refs. 1 and 2 to encompass chips-deformed-after separation. Hence, we may take that the analyses presented in Refs. 1 and 2 have also been verified, albeit indirectly.

Experiments conducted using a specially designed grooved tool to impose a predetermined side curl on the chip have yielded side-curl radii that are in good agreement with the theoretical prediction.

The new theory has focused only on the geometric transformations that take place during the development of a chip form. The geometric insights thus derived need to be integrated through an approach that also recognises the loads acting on the chip at the tool–chip and obstacle–chip contact areas and considers the stresses and strains present inside the whole chip body during obstacle–chip interaction. All this requires significant further research.

## Acknowledgements

This paper has been made possible by the funding (SRG 7001045) received from the Research Grants Council of Hong Kong for the second author's project on the geometric modelling of chip formation and chip forms.

## References

[1] A. Kharkevich, P.K. Venuvinod, Basic geometric analysis of 3-D chip forms in metal cutting. Part 1: determining up-curl and side-curl radii, Int. J. Machine Tools Manufact. 39 (5) (1999) 751–769.

[2] A.G. Kharkevich, P.K. Venuvinod, Basic geometric analysis of 3-D chip forms in metal cutting. Part 2: implications, Int. J. Machine Tools Manufact. 39 (6) (1999) 965–983.

[3] A.J. Pekelharing. Why and how does the chip curl and break? Ann CIRP 12 (3) (1963/64) 144–147.

[4] C. Spaans The fundamentals of three-dimensional chip curl, chip breaking and chip control. Doctor-thesis, TH-Delft, 1971.

[5] K. Nakayama, M. Ogawa, Basic rules on the form of chip in metal cutting, Ann. CIRP 27 (1) (1978) 17–21.

[6] K. Nakayama, M. Arai, Comprehensive chip form classification based on the cutting mechanism, Ann. CIRP 41 (1) (1992) 71–74.

[7] J. Shinozuka, T. Obikawa, T. Shirakashi, Chip breaking analysis from viewpoint of the optimum cutting tool geometry design, J. Mater. Process. Technol. 62 (1996) 345–351.

[8] R. Ghosh, O.W. Dillon Jr., I.S. Jawahir, An investigation of 3-D curled chip in machining. Part 1: A mechanics-based analytical model, Machining Sci. Technol. 2 (1) (1998) 91–116.

[9] R. Ghosh, O.W. Dillon Jr., I.S. Jawahir, An investigation of 3-D curled chip in machining. Part 2: Simulation and validation using FE techniques, Machining Sci. Technol. 2 (1) (1998) 117–135.

[10] M. Masuda, Y. Chujo, T. Hara, H.S. Qiao, Studies on the chip control in metal cutting (2nd Report). Estimation of the chip curl based on the side flow, J. Soc. Precision Eng. 53 (4) (1987) 558–564.

[11] E.K. Henriksen, Chip-breaker dimensions are critical in taming chips, Am. Machinist 98 (3) (1954) 118–124.

[12] S. Hilbert, Cohn-Vossen, Geometry and the imagination, Chelsea Publishing Company, New York, 1983.

[13] D.W. Henderson, Differential geometry, Prentice Hall, New Jersey, 1998.

[14] M.M. Lipschutz, Schaum's outline of theory and problems of differential geometry, McGraw-Hill, New York, 1969.

[15] R.S. Hahn, Some observations on chip curl in the metal-cutting process under orthogonal cutting conditions, Trans. ASME (J. Manufact. Sci. Eng.) 71 (1953) 581–590.

[16] P. Albrecht, New development in the theory of the metal-cutting process, J. Eng. Ind. November (1961) 557–571.

[17] C.A. van Luttervelt, Chip formation in machining operation at small diameter, Ann. CIRP 25 (1) (1976) 71–76.

[18] B. Ostle, L.C. Malone, Statistics in research, Iowa State University Press, Ames, IA, 1988.